Rotary-Atomizer Electric Power Generator

Trieu Nguyen,[1] Tuan Tran,[2] Hans de Boer,[1] Albert van den Berg,[1] and Jan C. T. Eijkel[1,*]

[1]*BIOS Lab on a Chip Group, MESA+ Institute for Nanotechnology, MIRA Institute for Biomedical Technology and Technical Medicine, University of Twente, Netherlands*

[2]*School of Mechanical and Aerospace Engineering, Nanyang Technological University, 50 Nanyang Avenue, Singapore 639798, Singapore*

(Received 28 November 2014; published 16 March 2015)

We report experimental and theoretical results on a ballistic energy-conversion method based on a rotary atomizer working with a droplet acceleration-deceleration cycle. In a rotary atomizer, liquid is fed onto the center of a rotating flat surface, where it spreads out under the action of the centrifugal force and creates "atomized" droplets at its edge. The advantage of using a rotary atomizer is that the centrifugal force exerted on the fluid on a smooth, large surface is not only a robust form of acceleration, as it avoids clogging, but also easily allows high throughput, and produces high electrical power. We successfully demonstrate an output power of 4.9 mW and a high voltage up to 3120 V. At present, the efficiency of the system is still low (0.14%). However, the conversion mechanism of the system is fully interpreted in this paper, permitting a conceptual understanding of system operation and providing a roadmap for system optimization. This observation will open up a road for building power-generation systems in the near future.

DOI: 10.1103/PhysRevApplied.3.034005

I. INTRODUCTION

Since its introduction in 1964 by Osterle [1], energy conversion from streaming current has been extensively explored, especially in the last 20 years, thanks to the rapid development of micro- and nanofabrication methods [2]. The streaming current mechanism can be described as follows. When a glass surface is in contact with aqueous solutions, it bears a negative charge due to ionization of surface silanol groups. Counterions will be attracted from the adjacent solution, forming an electrical double layer (EDL) with a net positive charge. The mobile counterionic charges in the diffuse part of the EDL are transferred if the solution is driven by an external force. Figure 1(a) shows such a conventional single-phase pressure-driven flow system. The resulting electrical current is called the streaming current (I_s). The downstream accumulation of ionic charges creates an electrokinetic (streaming) potential which acts to drive a current in the opposite direction to the streaming current called the conduction current (I_c). The net current is the difference between the streaming current and conduction current and can be directed to an external load to generate electrical power. Both the conduction current reducing the net current and the high hydrodynamic friction limit the efficiency of this pressure-driven single-phase (liquid) system [Fig. 1(a)] [3–7]. Classically experimental efficiencies were limited to 5% [8], but recently, efficiencies up to 46% were mentioned in highly charged membranes

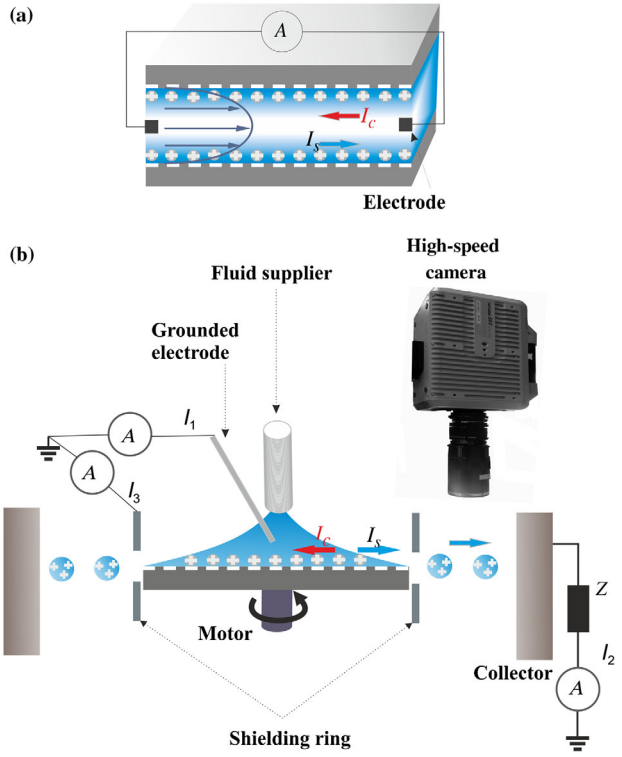

FIG. 1. (a) Single-phase conventional pressure-driven flow. I_s, streaming current; I_c, conduction current. (b) Schematic view of our approach using centrifugal force in a two-phase system. We denote the electrical current through the load resistor (Z) as I_2. The current is supplied from the grounded central electrode at the fluid supplier and denoted as I_1. A small amount of charged droplets will also land on the shielding ring. This electrical current is denoted as I_3.

*j.c.t.eijkel@utwente.nl

[9]. Also recently, ballistic microfluidic energy conversion was introduced by Xie *et al.* [10], converting mechanical to electrical energy by an acceleration-deceleration cycle of high-speed charged droplets launched through a membrane micropore, largely avoiding conduction-current generation and much increase in efficiency (up to 50%). However, all these methods use porous membranes, which are subject to the risk of clogging and require high-quality filtering. Here, instead of using a membrane pore, we report ballistic energy conversion using a rotary atomizer. Figure 1(b) shows the configuration of our two-phase (liquid and air) power-generation system based on a glass rotary atomizer and demineralized water. Ballistic energy-conversion systems such as presented by Xie *et al.* [10] and in the paper here use a two-phase configuration in which a two-step conversion mechanism occurs. First, we convert mechanical energy to kinetic energy of the air-isolated droplets and then the droplets' kinetic energy to electrical energy. This mechanism gives an elegant simultaneous demonstration of two fundamental laws of physics: the law of energy conservation and Newton's second law of motion, as we will show.

II. METHODS

A. Glass rotary atomizer

Figure 2 shows the schematic of the device structure. The motor model YM-261A-9 is supplied from Rakuten (Germany). The motor rotational speed is controlled by a voltage regulator. The rotational speed of the atomizer is measured by two different methods: (i) Fastscan SA-X (Photron, Japan) and (ii) ACT-3X tachometer by Monarch Instruments coupled to a remote optical sensor [11] (Monarch Instruments, model ROS-5W, USA). Droplet velocity and droplet size are analyzed using IMAGEJ [12] version 1.46r. A glass Petri dish (Fisher Scientific) connected to the top of the motor functions as the rotating plate.

B. Electrical measurement

The currents I_1, I_2, and I_3 are measured using Keithley instruments, namely, Keithley models 6487, 6485, 2410, respectively. Resistors with a voltage rating of 20 kV are used with varying values from 0.1 to 5 GΩ. The electrical potential of the charge collector is calculated following ohm's law $V = I_2 Z$. The resistors are immersed in insulating oil (Shell Diala S2-ZU-I) to prevent electrical losses by

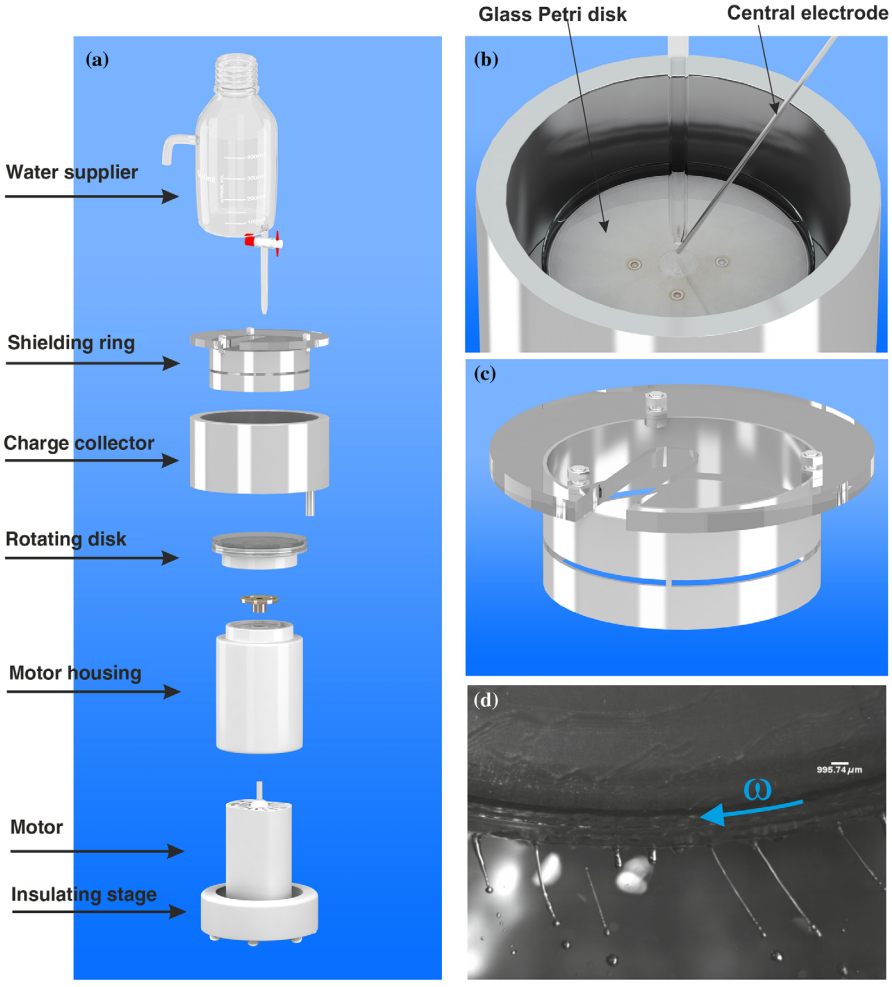

FIG. 2. (a) Exploded view of the atomizer setup. (b) Top view of the atomizer setup. (c) Schematic of the shielding ring. (d) Example of high-speed camera images obtained from our experimental measurement [captured using Fastscan SA-X (Photron, Japan)] at rotational speed 152 rad/s, volume flow rate 5 ml/s. The droplets formed are spherical.

discharge. All experiments are performed in air at atmospheric pressure and ambient temperature.

III. RESULTS

A. Microsized charged droplets

The exploded view and the top view of the glass rotary atomizer are shown in Figs. 2(a) and 2(b), respectively. Demineralized water is gravitationally supplied from a supplier bottle where the water level is kept constant by using an overflow valve. Upon contacting the center of the rotating glass Petri dish, the water is outwardly accelerated. The manner in which droplets are produced is dependent on six quantities: the dish diameter, rotary speed, liquid flow rate, surface tension, viscosity, and liquid density [13]. Disintegration of the continuous water layer on the Petri dish occurs when surface tension and viscous forces are overcome by the centrifugal forces. It has been established in the literature that droplets are produced by one of three operational modes, namely, direct droplet mode, ligament mode, and sheet mode [13,14]. In the ligament mode, stable liquid ligaments are formed at the dish circumference and disintegrate into droplets. In this work, the spinning dish is maintained at ligament operation mode to ensure the highest uniformity of droplets and minimal droplet size [13,15]. Once formed, driven by inertia, these droplets travel toward and land on the aluminum collector. Electrically, the ionic charges from the mobile part of the EDL on the Petri dish surface are transferred into the flying droplets and then electrochemically converted to an electron current at the aluminum collector. This electrical current (I_2) then passes through a load resistor (Z) connected to ground finally generating electrical power. To complete the circuit, the charges in the EDL are replenished by a current flowing through the grounded central electrode immersed in the solution supplied to the center of the disk [Fig. 1(b)]. A metal shielding ring having an opening of 4 mm and being electrically grounded is placed 1.5 mm from the rotating disk to shield the solution from electrostatic induction from the high potential of the charge collector, which is generated when resistors are used [as depicted in Fig. 2(c)]. The ring can also be used to induce extra charge on the droplets by applying a negative potential to it. The typical droplet sizes and velocities of the captured droplets are shown in Fig. 3(a) obtained at a rotational speed of 720 rad/s and a volume flow rate of 2.7 ml/s. The droplet size distribution can be fitted well with the log-normal function [see Fig. 3(b)]. This result is in agreement with the literature for rotary-atomizer systems [16].

B. Streaming current and output power

Power is harvested by the load resistor. We denote the electrical current through the load resistor as I_2. Current supplied from the grounded electrode at the fluid supplier is denoted as I_1. A small amount of charged droplets will also land on the shielding ring and generate an electrical current denoted as I_3 [see Fig. 1(b)]. Figures 4(a) and 4(b) show the electrical currents I_1, I_2, I_3 with [4(a), $I_3 > 0$] and without [4(b), $I_3 = 0$] the use of the grounded shielding ring. The current I_1 represents the sum of the streaming current and conduction current ($I_1 = I_s + I_c$). The current I_2 equals I_1 minus losses of charged droplets. The generated target voltage ($V = I_2 Z$) and output power ($P_{\text{out}} = VI_2$) in both cases, with and without use of the grounded shielding ring, are depicted in Figs. 5(a) and 5(b).

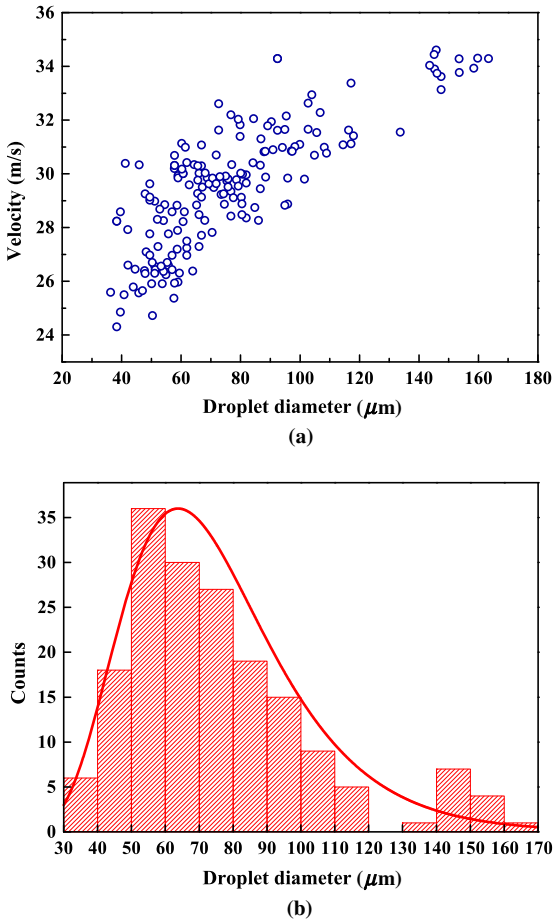

FIG. 3. (a) Droplet size versus droplet velocity. (b) Droplet size distribution (bars) fitted with a log-normal distribution (line). Experiments are performed at angular velocity $\omega = 720$ rad/s and flow rate $Q = 2.7$ ml/s.

IV. DISCUSSION

From Figs. 4(a) and 4(b), it is clearly seen that without the shielding ring, the currents I_1 and I_2 both decrease with an increase of load resistor value and that I_2 is approximately equal to I_1. In this case, the increase of the load resistor value leads to an increase of the target potential and thereby increases the conduction current via an inductive

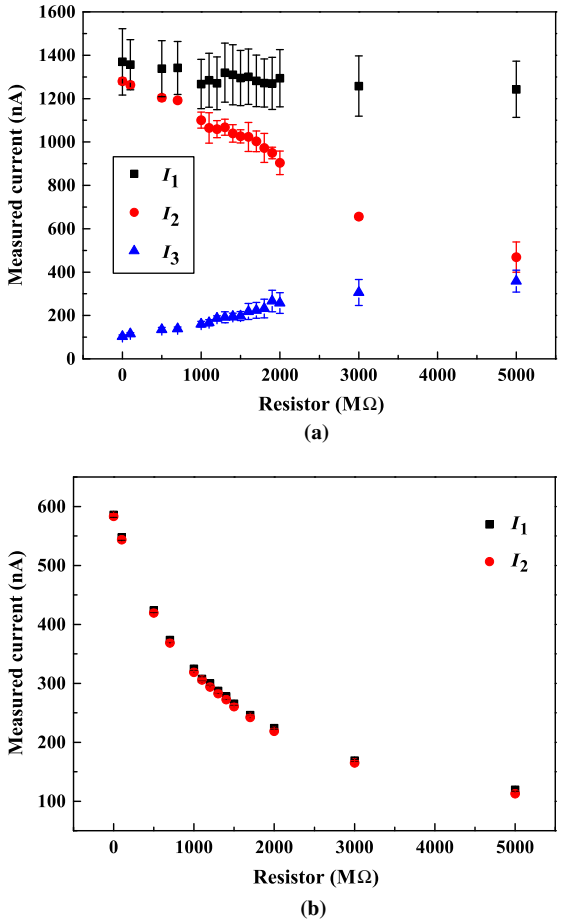

FIG. 4. Measured current versus resistor values with (a) and without (b) using the grounded shielding ring.

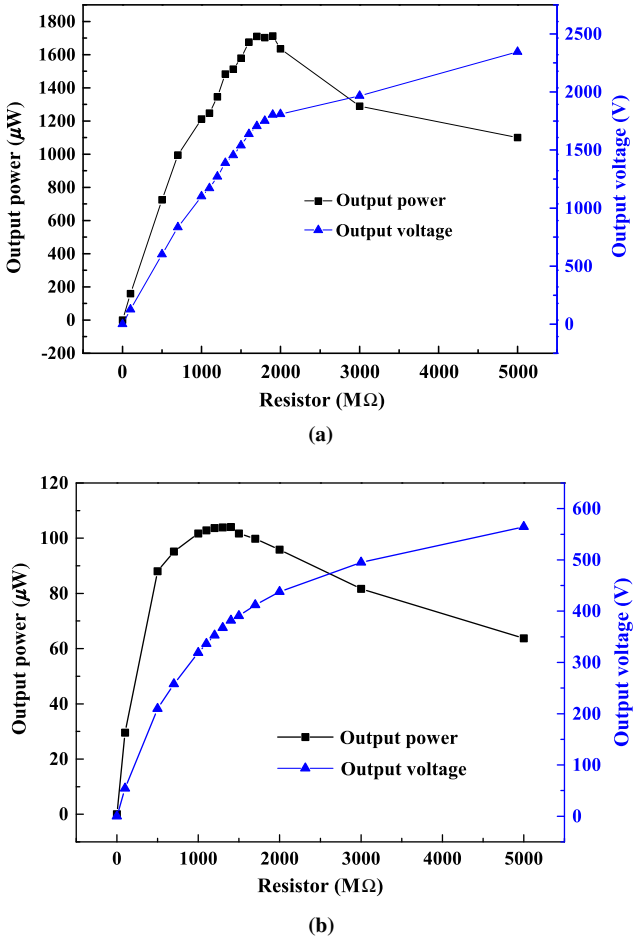

FIG. 5. Output power and output voltage with (a) and without (b) using the grounded shielding ring. Experiments are performed using demineralized water at *p*H 6.

mechanism, reducing I_1 and thereby I_2. This induction occurs at the water-air interface through a continuously distributed resistance and capacitance as formed by the aqueous solution and its interface with the air [17,18]. It is obvious from Figs. 4(a) and 4(b) that the use of the grounded shielding ring prevents induction and, hence, the reduction of I_1 which now remains constant for load resistors up to $R = 1900$ MΩ (target potential up to 2 kV), though at the cost of an increasing current loss I_3. With load resistor values higher than 1900 MΩ, $I_1 \geq I_2 + I_3$, and we assume current is lost to other processes such as the electrical breakdown at high target voltage ($V > 2.5$ kV).

When no load resistor is used, an increase of both I_1 and I_2 is seen in the case where the grounded shielding ring is used when compared to the case without the shielding ring (from 600 to 1400 nA; Fig. 4). We hypothesize that this increase is caused by the change of the electrical potential at the location of the grounded ring from strongly positive in its absence (due to the generated streaming potential) to ground potential when present. In the former case, a strong conduction current will be generated, decreasing I_1, while in the latter case, the conduction current will be much smaller. This hypothesis can be demonstrated by using the method of image charges (please refer to the Supplemental Material [19] and Ref. [20]).

The maximum output power we can generate with the grounded shielding ring is 1.7 mW [as shown in Fig. 5(a)]. In order to further increase the charge on the droplets and the output power, we apply a negative potential to the shielding ring making it an induction electrode, attracting positive charges to the water-air interface. This induction charging occurs at the water-air interface through a continuously distributed resistance and capacitance as formed by the aqueous solution and its interface with the air. As the jets break up, the droplets retain the induced charge. We apply a voltage of −1 kV in the experiments reported here. It is clearly seen from Fig. 6(a) that for $Z = 0$ MΩ, the current I_1 now is 3074 nA, which is 2 times larger than in the case of the grounded shielding ring [1400 nA; Fig. 4(a)] and can be contributed to the charge induction mechanism. The maximal output power we obtain for the case of applied negative potential to the shielding ring is

4.9 mW [Fig. 6(b)] at an output voltage of 3120 V. The energy-conversion efficiency of the system (χ) is defined by the ratio between the electrical output power (P_{out}) and the mechanical input power (P_{in}),

$$\chi = \frac{P_{\text{out}}}{P_{\text{in}}} = \frac{I_2 V}{\tau\omega} = \frac{I_2 V}{\dot{M} v_0^2}. \quad (1)$$

In this equation, $\tau = \dot{M} v_0 R_e$ is the torque [21] required to rotate the glass dish excluding all loss sources except water acceleration. $\dot{M}$ is the mass flow rate. The tangential velocity is $v_0 = \omega R_e$. R_e is the radius of the rotating dish, and ω is the angular velocity. For details on the derivation of the equation for the input power and its components, please refer to the Supplemental Material [19] and Refs. [22–24]. For the current experiments with rotational speed $\omega = 720$ rad/s, $v_0 = 36$ m/s, the energy-conversion efficiency of the system calculated from Eq. (1) is 0.14%.

In the following, we will discuss the conversion mechanism, the energy-conversion efficiency of the system, and the way to optimize the system to maximize conversion efficiency. In order to achieve clarity in the analysis, we divide our atomizer generator process into four component steps: (1) water feeding, (2) charging and accelerating, (3) droplet formation and transport, and (4) droplet landing and charge transfer (Fig. 7). Charging of the droplets occurs at step 2 by double-layer advection and induction. In step 2, we also accelerate the liquid by frictional coupling between the solid surface and the liquid mass. This process is a high-loss coupling, with the loss determined by the internal friction in the liquid during the acceleration. The entire invested energy (P_{in}) will, thus, be the sum of the final (liquid) kinetic energy (P_k) and the frictional losses ($P_{f,\text{liq}}$). As mentioned in the Supplemental Material [19], the frictional losses $P_{f,\text{liq}}$ cost 50% of the input power. The other 50% of the input power goes to the kinetic energy of the water (P_k) leaving from the dish edge. In step 3, droplets are formed and transported towards the target through the air. As shown in the Supplemental Material [19], the energy needed for surface creation can be neglected. The theoretical maximum conversion efficiency will be less than 50% by taking into account the energy loss in step 3 due to the air friction. In the Supplemental Material [19], we show that under the present operating conditions, the air friction consumes 33% of the droplet kinetic energy. At step number 4, the charged droplets land on the collector, charging it up to a steady-state potential $V = I_2 Z$. The potential V gives rise to an electrical field $\vec{E}$ and droplet (i) with charge q_i by its kinetic energy has to overcome the electrical force $\vec{E} q_i$ to land on the collector. From Newton's second law for droplet mass (m_i) and acceleration $\vec{a}$, $\vec{F} = m_i \vec{a}$, we obtain the force balance on an individual droplet i,

$$m_i \vec{a} = -\vec{E} q_i. \quad (2)$$

Now we assume that the surface charge density is equal for all droplets and independent of their size. The charge-to-mass ratio of individual droplets $(q/m)_i$ then is [25] (for derivation and nomenclature, see the Supplemental Material [19] and Refs. [26–29])

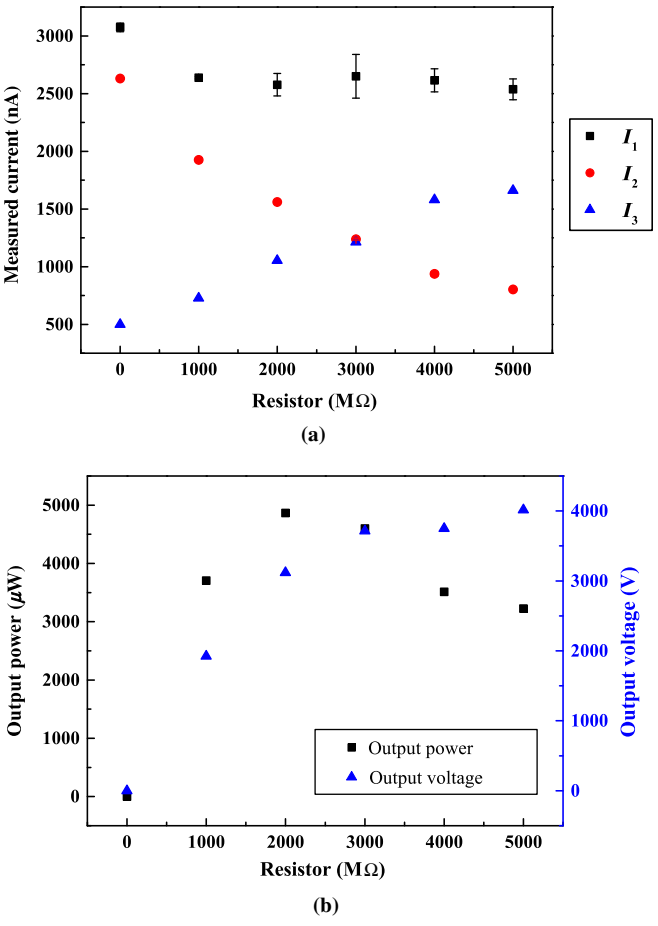

FIG. 6. (a) Measured current and (b) calculated output power and output voltage versus resistor values when −1 kV is applied to the shielding ring.

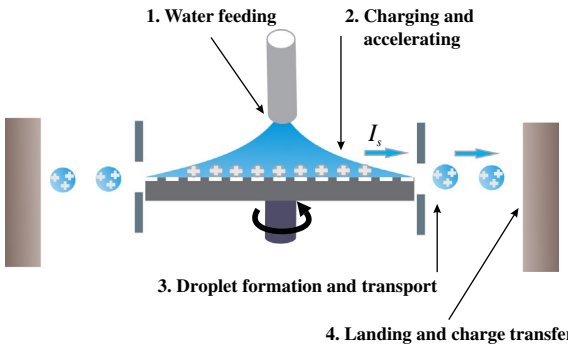

FIG. 7. Component steps of the rotary-atomizer generator.

$$\left(\frac{q}{m}\right)_i = \frac{I_1}{r_i \dot{M}} \frac{\sum_i^n n_i r_i^3}{\sum_i^n n_i r_i^2}. \quad (3)$$

The maximal energy-conversion efficiency of the system for droplet i now is obtained when the droplet kinetic energy $(m_i v_i^2/2)$ equals the generated electrical potential energy $(q_i V)$,

$$\chi_{\max_i} = 0.5\left(\frac{q_i V}{\frac{1}{2} m_i v_i^2}\right), \quad (4)$$

where the factor 0.5 stems from the energy loss in step 2. Droplet velocity at landing then equals zero, and no energy is lost to collision.

By substituting $(q/m)_i$ from Eq. (3) into Eq. (4),

$$\chi_{\max_i} = \left(\frac{I_1}{\dot{M}}\right)\left(\frac{V}{v_i^2}\right)\left(\frac{\sum_i^n n_i r_i^3}{r_i \sum_i^n n_i r_i^2}\right). \quad (5)$$

Equation (5) is identical to Eq. (1) if the following conditions are satisfied:

(a) the droplet size distribution is monodisperse $(\frac{\sum_i^n n_i r_i^3}{r_i \sum_i^n n_i r_i^2} = 1)$,

(b) the droplet velocity is equal to the rotating tangential velocity $(v_i = v_0)$, meaning no loss due to air friction, and

(c) $I_2 = I_1$, meaning no current loss by leakage to the shielding ring.

Figure 8 shows the theoretical maximum energy-conversion efficiency for individual droplets plotted from Eq. (5), in which v_i and r_i are the measured droplet velocity and droplet radius (when droplets pass through the shielding ring, 3 mm from the dish edge), implying that no droplet loss occurs and V is 3.12 kV. It is obvious that from the smaller droplet sizes with a higher charge-to-mass ratio [please refer to the Supplemental Material [19] for $(q/m)_i = C(1/r_i)$], larger energy-conversion efficiencies can be obtained. However, even for the smallest droplets of 20-μm radius, only a small fraction of the kinetic energy (3.2% at an overall efficiency of 1.6%) can be harvested at the target potential of 3.12 kV. Theoretically, one can obtain overall maximum conversion efficiency of the system at $(100\%–50\%) \times (100\%–33\%) = 33.5\%$ when all droplet kinetic energy is converted to electrical energy (with 33% loss of kinetic energy to the air friction). To obtain this optimal conversion, droplets need to be maximally decelerated, which occurs when $\vec{a} = -\vec{E}\frac{q_i}{m_i}$ [from Eq. (2)] is maximized. Further increasing the charge-to-mass ratio $(\frac{q_i}{m_i})$, therefore, is crucial as this increase will allow harvesting a larger proportion of the kinetic energy, which is now lost on droplet impact. Our present droplet mean charge-to-mass ratio is still less than 13 times that of the Rayleigh limit [30] $[q_{\max} = (8\pi^2 \varepsilon^0 \sigma d^3)^{0.5}]$, implying the electrical force at the same target potential can still be increased by at least 1 order of magnitude if the charge-to-mass ratio can be efficiently increased. It is obvious that in the future work, decreasing the droplet size as well as increasing the monodispersity have to be the aim, coupled to an efficient charge induction, so that higher conversion efficiencies can be obtained. One of the ways to obtain a smaller and more uniform droplet size is to reduce the volume flow rate of the system (in case we decide to maintain the other liquid properties) since it was shown [14] that the mean droplet size d_{mean} is proportional to Q, $d_{\text{mean}} = Q^\alpha f(\omega, R_e, \sigma, \rho, \mu)$. Here, α is a positive constant (always >0.1), which is dependent on the atomization modes. Consider the future use of liquids other than water; the liquid of choice should allow a maximal charge-to-mass ratio. The density should, therefore, be low while the Rayleigh limit indicates the surface tension should be high. Furthermore, the effect of liquid properties such as viscosity and density on droplet size as mentioned in the formula above should be considered. A fundamentally different centrifugal ballistic system could also be envisaged, based on using nonconducting liquids coupled to charge injection from a conducting plate. Finally, as can be seen in Eq. (4), increasing the target voltage is another aim, as this gain will increase the electrical field $\vec{E}$ [in Eq. (2)] and, hence, deceleration. At present, we find the target voltage is limited to 3.12 kV due to spontaneous discharge.

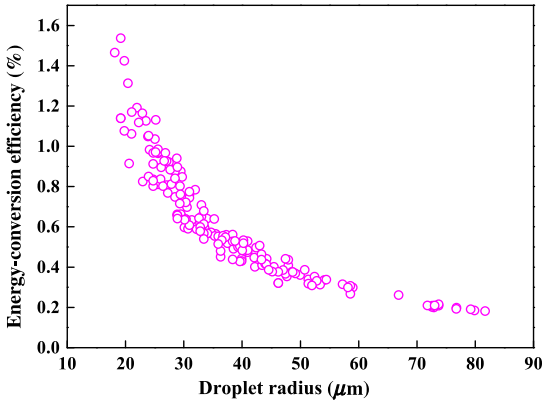

FIG. 8. Theoretical maximum energy-conversion efficiency from experimentally determined droplet sizes and velocities at a target potential of 3.12 kV and no droplet loss (i.e., maximum efficiency at $I_2 = I_1$).

V. CONCLUSIONS

To conclude, we show an approach to generate electrical energy from a rotary-atomizer system. The principle demonstrated is extremely simple, as it needs only water, a rotating disk, and a metal droplet collector. The rotary-atomizer generator presented in this work, interestingly, is the opposite process of electrospraying, which is used, e.g.,

in rotary atomizers for electrostatic painting and crop-dusting applications, and where a high voltage is needed to generate charged droplets. Apart from being an energy-generation method, our approach opens up a way for charging droplets from which applications requiring either charged droplets, a rotary atomizer, or both, such as electrostatic painting and crop dusting, can benefit.

ACKNOWLEDGMENTS

The authors thank Dr. Yanbo Xie for fruitful discussion on the electrical circuit. Johan Bomer is gratefully acknowledged for the technical support. Hivolt.de (GmbH & Co. KG, Hamburg, Germany) is thanked for supporting with high-voltage cable. The project is financially supported by a Nederlandse Organisatie voor Wetenschappelijk (NWO) TOP Grant No. 700.58.341, Netherlands.

[1] J. F. Osterle, Electrokinetic energy conversion, J. Appl. Mech. **31**, 161 (1964).
[2] Sumita Pennathur, Jan C. T. Eijkel, and Albert Berg van den, Energy conversion in microsystems: Is there a role for micro/nanofluidics?, Lab Chip **7**, 1234 (2007).
[3] Frank H. J. van der Heyden, Douwe Jan Bonthuis, Derek Stein, Christine Meyer, and Cees Dekker, Electrokinetic energy conversion efficiency in nanofluidic channels, Nano Lett. **6**, 2232 (2006).
[4] Frank H. J. van der Heyden, Douwe Jan Bonthuis, Derek Stein, Christine Meyer, and Cees Dekker, Power generation by pressure-driven transport of ions in nanofluidic channels, Nano Lett. **7**, 1022 (2007).
[5] T. Nguyen, Y. B. Xie, L. J. de Vreede, A. van den Berg, and J. C. T. Eijkel, Highly enhanced energy conversion from the streaming current by polymer addition, Lab Chip **13**, 3210 (2013).
[6] Wouter Olthuis, Bob Schippers, Jan Eijkel, and Albert Berg van den, Energy from streaming current and potential, Sens. Actuators B Chem. **111–112**, 385 (2005).
[7] Yanbo Xie, John D. Sherwood, Lingling Shui, Albert van den Berg, and Jan C. T. Eijkel, Strong enhancement of streaming current power by application of two phase flow, Lab Chip **11**, 4006 (2011).
[8] Yanbo Xie, Xinwei Wang, Jianming Xue, Ke Jin, Long Chen, and Yugang Wang, Electric energy generation in single track-etched nanopores, Appl. Phys. Lett. **93**, 163116 (2008).
[9] S. Haldrup, J. Catalano, M. R. Hansen, M. Wagner, G. V. Jensen, J. S. Pedersen, and A. Bentien, High electrokinetic energy conversion efficiency in charged nanoporous nitrocellulose/sulfonated polystyrene membranes, Nano Lett. **15**, 1158 (2015).
[10] Yanbo Xie, Diederik Bos, Lennart J. de Vreede, Hans L. de Boer, Mark-Jan van der Meulen, Michel Versluis, Ad J. Sprenkels, Albert van den Berg, and Jan C. T. Eijkel, High-efficiency ballistic electrostatic generator using microdroplets, Nat. Commun. **5**, 3575 (2014).
[11] Heather D. Willauer, Ramagopal Ananth, John B. Hoover, George W. Mushrush, and Frederick W. Williams, Critical evaluation of rotary atomizer, Petrol. Sci. Technol. **24**, 1215 (2006).
[12] C. A. Schneider, W. S. Rasband, and K. W. Eliceiri, Nih image to imagej: 25 years of image analysis, Nat. Methods **9**, 671 (2012).
[13] A. R. Frost, Rotary atomization in the ligament formation mode, Journal of Agricultural Engineering Research **26**, 63 (1981).
[14] Y. Tanasawa, Y. Miyasaka, and M. Umehara, Effect of shape of rotating disks and cups on liquid atomization, in *Proceedings of the 1st International Conference on Liquid Atomization and Spray Systems, Tokyo, 1978*, (Fuel Society of Japan, Tokyo, 1979) pp. 165–172.
[15] Kenneth D. Kihm, B. H. Kim, and A. R. McFarland, Atomization, charge, and deposition characteristics of bipolarly charged aircraft sprays, Atomization Sprays **2**, 463 (1992).
[16] Ghasem G. Nasr, Andrew J. Yule, and Lothar Bendig, *Industrial Sprays and Atomization: Design, Analysis and Applications* (Springer, New York, 2002), p. 491.
[17] Yanbo Xie, Ph.D. thesis, University of Twente, 2013.
[18] A. Atten and S. Oliveri, Charging of drops formed by circular jet breakup, J. Electrost. **29**, 73 (1992).
[19] See the Supplemental Material at http://link.aps.org/supplemental/10.1103/PhysRevApplied.3.034005 for details on the theoretical solution for the main paper.
[20] David Keun Cheng, *Field and Wave Electromagnetics* (Addison-Wesley, New York, 1989), Vol. 2.
[21] James O. Wilkes, *Fluid Mechanics for Chemical Engineers* (Prentice-Hall, Englewood Cliffs, NJ, 2006), p. 91.
[22] A. F. Charwat, R. E. Kelly, and C. Gazley, The flow and stability of thin liquid films on a rotating disk, J. Fluid Mech. **53**, 227 (1972).
[23] Tharwat F. Tadros, *Surfactants in Agrochemicals* (Marcel Dekker, New York, 1995), p. 219.
[24] R. L. C. Flemmer and C. L. Banks, On the drag coefficient of a sphere, Powder Technol. **48**, 217 (1986).
[25] Nikola Toljic, Ph.D. thesis, The University of Western Ontario, 2012.
[26] Joshua L. Hensley, Xin Feng, and James E. Bryan, Induction charging nozzle for flat fan sprays, J. Electrost. **66**, 300 (2008).
[27] Manoj Kumar Patel, C. Ghanshyam, and Pawan Kapur, Characterization of electrode material for electrostatic spray charging: Theoretical and engineering practices, J. Electrost. **71**, 55 (2013).
[28] J. E. Mccarthy, Jr. and D. W. Senser, Specific charge measurements in electrostatic air sprays, in *Proceedings of the Industry Applications Society Annual Meeting* (IEEE, 1993), Vol. 3, pp. 1905–1910.
[29] Nikola Toljic, K. Adamiak, G. S. P. Castle, Hong-Hsiang Kuo, and Hua-Tzu Fan, Three-dimensional numerical studies on the effect of the particle charge to mass ratio distribution in the electrostatic coating process, J. Electrost. **69**, 189 (2011).
[30] A. Gomez and K. Q. Tang, Charge and fission of droplets in electrostatic sprays, Phys. Fluids **6**, 404 (1994).